



# Mass-based hybridity model for thermomicro-polar binary nanofluid flow: first derivation of angular momentum equation

Mahmoud Behrouz<sup>a</sup>, Saeed Dinarvand<sup>a,\*</sup>, Mohammad Eftekhari Yazdi<sup>a</sup>,  
Hossein Tamim<sup>b</sup>, Ioan Pop<sup>c</sup>, Ali J. Chamkha<sup>d</sup>

<sup>a</sup> Department of Mechanical Engineering, Central Tehran Branch, Islamic Azad University, Tehran, Iran

<sup>b</sup> Department of Mechanical Engineering, Arak Branch, Islamic Azad University, Arak, Iran

<sup>c</sup> Department of Mathematics, Babes-Bolyai University, Cluj-Napoca 400084, Romania

<sup>d</sup> Faculty of Engineering, Kuwait College of Science and Technology, Doha District, 35004, Kuwait

## ARTICLE INFO

### Keywords:

Thermomicro-polar binary nanofluid  
Mass-based model  
Fraction-based model  
Microrotation  
Mixed convection

## ABSTRACT

The flow of thermomicro-polar binary nanofluid upon a perpendicular permeable shrinking sheet with the mixed convective effects in attendance of a lateral magnetic field is numerically explored. The framework and novelty of this work is a one-phase hybrid nanofluid model (Tiwari-Das model) using a unique mass-based technique that proposes base liquid mass, first and second solid-particle masses as essential inputs to acquire the main thermophysical characteristics of hybrid nanofluid. The alumina and copper solid-particles are dispersed in water as the base liquid and have a spherical form. The dominating dimensional PDEs are changed using the similarity transformation approach to a system of non-dimensional ODEs. This system is solved by utilizing *bvp4c* in the Matlab package. The values of the shear stress, the microrotation gradient, and heat transfer for three cases (i.e. pure thermomicro-polar fluid, thermomicro-polar nanofluid, and thermomicro-polar binary nanofluid) are gained and analyzed with formerly reported cases to validate our computational method. The influence of the emerging parameters on the velocity, angular velocity, temperature distribution, shear stress, the microrotation gradient, and the heat transfer of the thermomicro-polar binary nanofluid is reported and analyzed by the tabular and graphical results. It is found that heat transfer, shear stress, and microrotation gradient first augment and then reduce with the enhancement of the shrinking parameter. Adding the second nanoparticle has a positive effect on heat transfer; although its increasing effect (unfavorable) also on skin friction should be considered in engineering applications. The reliable implementation of the mass-based model for the thermomicro-polar binary nanofluid flow and the heat transfer is a significant accomplishment of the current research while the specific findings have been provided and argued in the body of the article.

## 1. Introduction

Water, ethylene glycol, refrigerants, biofluids, polymeric solutions oils, and lubricants are common base liquids that have significant limitations in increasing the effectiveness of several technical devices, including heat exchangers and electrical equipment [1–4].

\* Corresponding author.

E-mail addresses: [sae.dinarvand@iauctb.ac.ir](mailto:sae.dinarvand@iauctb.ac.ir), [saeed\\_dinarvand@yahoo.com](mailto:saeed_dinarvand@yahoo.com) (S. Dinarvand).

<https://doi.org/10.1016/j.cjph.2023.03.006>

Received 16 December 2022; Received in revised form 13 February 2023; Accepted 2 March 2023

Available online 7 March 2023

0577-9073/© 2023 The Physical Society of the Republic of China (Taiwan). Published by Elsevier B.V. All rights reserved.

## Nomenclature

A	shrinking parameter
B	microinertia parameter
$B_0$	magnetic ground strength
c	constants
C	heat capacity
$C_f$	skin friction coefficient
$C_p$	specific heat at constant pressure
D	coefficient of micropolar heat conduction
g	acceleration due to gravity
h	coefficient of convective heat transfer
hp	hybrid particle
j	micro-inertia density
k	thermal conductivity
K	material parameter
m	mass
M	magnetic parameter
n	component of microrotation
N	microrotation in the xy plane
$Nu_x$	local Nusselt number
Pr	Prandtl number
R	radiation parameter
Ri	Richardson number
$Re_x$	local Reynolds number
S	suction or injection parameter
T	temperature field
u, v	velocity components along x and y axes
x, y	2D Cartesian coordinates system

### Greek symbols

$\phi$	volume fraction
$\beta$	coefficient of thermal expansion
$\eta$	independent similarity variable
$f(\eta)$	non-dimensional stream function
$\theta(\eta)$	dimensionless temperature distribution
$\mu$	dynamic viscosity
$\nu$	kinematic viscosity
$\rho$	Density
$\sigma$	electrical conductivity
$\gamma_1$ to $\gamma_6$	Coefficients of ODE equations
$\rho C_p$	volumetric heat capacity at constant pressure
$\kappa$	vortex viscosity
$\delta$	micropolar heat conduction parameter

### Subscripts

s	equivalent property of nanoparticles
f	base liquid
nf	mono-nanofluid
hmf	hybrid nanofluid
1	first nanoparticle ( $Al_2O_3$ )
2	second nanoparticle (Cu)
$\infty$	Conditions in the free stream
w	surface of the plate

Choi introduced the concept of using solid-particles in fluids in 1995, with the goal of increasing the thermal conductivity of the base liquid [5–7]. The traditional nanofluid models have significant restrictions. They are unable to explain a category of liquids with specific microscopic characteristics resulting from the microrotation and local structure of the liquid elements [8]. Nano particles in engineering applications range in size from 1 to 100 nm [9,10]. Nanofluids have demonstrated a great potential for increasing heat transmission rates in a variety of usages [11,12]. Hybrid nanofluid or nanocomposite fluid is a new type of nanofluid created by

suspending two various kinds of solid particles in a base liquid [1,5]. A hybrid nanoparticle is a substance that combines the chemical and physical characteristics of multiple solid-particles at the same time and delivers the characteristics in a homogeneous phase. Synthetic hybrid solid-particles have a considerable physicochemical feature that individual particles do not have [1]. In many engineering applications, such as solar technologies, electronics, microelectronics, instrumentation, heat exchangers, microfluidics, defense, transpiration cooling of gas-turbine blades, and thermal scalability, nanofluids and hybrid nanofluids can be used to improve the performance of systems or technologies in heat transfer subject. Porous plates have been utilized to mimic a number of surface phenomena, including fluid transfer in living organisms, propellant burning, phase sublimation, ablation cooling, and evenly distributed irrigation [7].

The influences of various solid-particle types and shapes on heat transfer, velocity, and angular velocity have been investigated [9, 11]. Copper and Alumina solid-particles with spherical forms are used in this study. Table 2 lists all of the physical characteristics in detail. These particles have been used in several studies by academics. In their assessment of contemporary research, development, and applications of hybrid nanofluids, Suresh et al. [14] employed these nonopartclcs and provided correlations for friction and Nusselt number for flow of alumina-copper solid-particles. It has also been observed that hybridizing metallic copper particles with alumina solid-particles significantly improved the effective thermal conductivity. When these particles were utilized in an exponentially decreasing sheet, Waini et al. [15] found that the rate of heat transfer and the skin friction increase.

The Newtonian fluid theory does not apply to fluids like lubricants, colloidal fluids, polymeric suspension, animal blood, man-made liquids with polymeric additives, biological fluids, yoghurt, tomato sauce, paints, grease, polymers, and so on. The micropolar fluid has drawn the most interest among all non-Newtonian fluids since it features an extra angular momentum equation. Eringen [16] is credited for creating the theory of micropolar fluids, which also introduced the classical Navier-Stokes equations and the equation of angular momentum.

The thermomicropolar fluids hypothesis was afterwards created by Eringen [17] by expanding this idea once more and accounting for the thermal influence. The dynamics of nanomicropolar fluids have been extensively modeled and studied in recent years by BVP researchers. Gorla [18] explored the flow by stagnation point upon mobile plate for the 2D boundary layer equations of a micropolar fluid. Similarity equations were derived by Jena and Mathur [19] for the thermomicropolar-fluid free-convective flow across a perpendicular wall. Jena and Mathur also analyzed how permeability affected the flow upon a sheet under nonlinear temperature circumstances [20]. Ishak et al. [21] explored the mixed convective boundary layer flow on a perpendicular sheet submerged in an incompressible micropolar fluid. Lund et al. [22], dinarvand et al. [2], and Shatanawi et al. [23] have all studied the numerical research of micropolar nanofluid across a linearly decreasing plate. In order to expose the flow characteristics of a micropolar nanofluid across a stretched sheet while taking into account the impacts of magnetic ground and viscous dissipation, Hsiao [24] performed numerical simulations. In an aqua nanofluid, Khan et al. [25] examine the triple effects of the Navier slip, the gyrotactic microorganisms as well as magnetic ground. It was found that the magnetic ground enhances the temperature in flow while suppressing the dimensionless velocity. Bhattacharyya et al. [26] looked at how thermal radiation affected the heat transfer and flow of micropolar fluid via a porous shrinking sheet. Al-Sanea [27] examined the flow and heat transmission characteristics of a vertical layer of extruded material that moves constantly. Industrial engineering and manufacturing procedures including metal extrusions, continuous glass casting, wire drawing, or other processes containing these sorts of surfaces have utilized boundary layer flow induced by the stretched or shrinking plate [28].

In common methods, thermophysical properties of nanofluid or hybrid nanofluid are formulated as a function of nanoparticle volume fraction (and other possible parameters). Therefore, obviously, the final governing equations include this parameter. Here, the approach is based on the single-phase Tiwari-Das hybrid nanofluid model, which considers the mass of base fluid and nanoparticle instead of nanoparticle volume fraction. Numerous studies have focused on fraction-based analyses of nanofluids and hybrid nanofluids, but Dinarvand [29] was the first to provide the mass-based approach. Besides, few research have focused on the analysis of the flow of thermomicropolar binary nanofluid across a diminishing plate, as Roy [30] pointed out, and he has done it in a fraction-based model. These descriptions justify the objective and motivation of the present work. The mass-based model has many advantages, such as ease of use and the ability to compute thermophysical parameters of thermomicropolar binary nanofluids using the masses of both base liquid and solid-particle. Finally, the goal of this work is to evaluate the flow of a thermomicropolar binary nanofluid across a diminishing plate by utilizing mass-based model, as stated in the above introduction. The problem's solutions are offered for several relevant parameters after the controlling equations are solved through Matlab software. This model suggests a fresh definition for density, specific heat, as well as the equivalent solid volume fraction. These quantities are generated from the simultaneous thermophysical characteristics of the base liquid and solid-particles.

## 2. Thermomicropolar binary nanofluid flow and mathematical formulation

The boundary layer flow induced by the stretching or shrinking plate is important in industrial engineering and manufacturing procedures including metal extrusions, continuous glass casting, wire drawing, and other processes. Besides the analysis of thermomicropolar is applicable to modeling biological fluids such as blood. A cumulative application that contains both stretching/shrinking surface and thermomicropolar subjects is blood flow in contact with the vessel wall. Moreover, two nanoparticles added to the base fluid (blood) can be components of a nano-based drug.

Assume a steady incompressible 2D quiescent fluid flow of a thermomicropolar binary nanofluid upon the shrinking plate while it is subjected to the influences of a uniform magnetic ground (BO) normal to the plate, as illustrated in Fig. 1. The y-axis is perpendicular to the surface's selected x-axis and runs along it. A little incision at the beginning causes problems on the plate.

Due to the abrupt move of the slit as well as the absence of any additional influences, we consider the fluid's characteristics are

constant and isotropic. It is assumed that the solid phase, which includes Alumina (Al<sub>2</sub>O<sub>3</sub>) and Copper (Cu), and the fluid phase, which is pure water, are in thermal equilibrium. The solid-particles and the base liquid features are also assumed to remain constant. When there is no slip between the solid-particles and the base liquid, the single-phase model is correct [31]. As a consequence, the fluid phase and solid phase of the working fluid are in complete thermal equilibrium, and as a result, the volume concentration of the solid-particles will be constant throughout the bulk fluid. Here, the second model is used to examine the thermal and dynamic characteristics of a binary nanofluid. The fundamental premise of this model is that the mixture exhibits the characteristics of a single phase fluid; hence, the nanofluid is viewed as a conventional fluid with improved characteristics as a result of the presence of solid-particles. Additionally, in accordance with our semi-analytical single phase model, copper is dispersed inside the nanofluid (as a new base liquid, Al<sub>2</sub>O<sub>3</sub>/water) in order to build the selective thermomicropolar binary nanofluid after the addition of alumina to the base liquid to create the nanofluid [9,22]. These factors, along with the standard Boussinesq approximation, allow us to formulate the boundary layer controlling equations for the thermomicropolar binary nanofluid, as follows [29,30,32,33]:

$$\frac{\partial u}{\partial x} + \frac{\partial v}{\partial y} = 0, \tag{1}$$

$$u \frac{\partial u}{\partial x} + v \frac{\partial u}{\partial y} = \frac{\mu_{hmf} + \kappa}{\rho_{hmf}} \frac{\partial^2 u}{\partial y^2} + \frac{\kappa}{\rho_{hmf}} \frac{\partial N}{\partial y} - g \frac{(\rho\beta)_{hmf}}{\rho_{hmf}} (T - T_\infty) - \frac{\sigma_{hmf} B_0^2}{\rho_{hmf}} u, \tag{2}$$

$$u \frac{\partial N}{\partial x} + v \frac{\partial N}{\partial y} = \frac{1}{\rho_{hmf}} \left( \mu_{hmf} + \frac{\kappa}{2} \right) \frac{\partial^2 N}{\partial y^2} - \frac{\kappa}{\rho_{hmf} j} \left( 2N + \frac{\partial u}{\partial y} \right), \tag{3}$$

$$u \frac{\partial T}{\partial x} + v \frac{\partial T}{\partial y} = \alpha_{hmf} \frac{\partial^2 T}{\partial y^2} + \frac{D}{(\rho C)_{hmf}} \left( \frac{\partial T}{\partial x} \frac{\partial N}{\partial y} - \frac{\partial T}{\partial y} \frac{\partial N}{\partial x} \right). \tag{4}$$

Restricted with the boundary conditions [30]

$$\begin{aligned} u &= Au_w(x), & v &= v_w(x), & N &= -n \frac{\partial u}{\partial y}, & T &= T_\infty + T_0 x & \text{at } y &= 0, \\ u &= 0, & N &= 0, & T &= T_\infty & \text{as } y &\rightarrow \infty. \end{aligned} \tag{5}$$

where  $T$  is the temperature of the fluid,  $T_\infty$  is the ambient temperature,  $u$  and  $v$  are the velocities in two directions,  $N$  is the micro-rotation,  $j$  is the micro-inertia density,  $g$  is the gravity acceleration,  $\kappa$  is the vortex viscosity and  $D$  is the coefficient of micropolar heat conduction in the above equations. In the boundary conditions  $u_w(x) = cx$  ( $c > 0$ ) is the shrinking sheet velocity related to on the parameter of shrinking ( $A < 0$ ),  $v_w(x)$  is related to the mass flux by the sheet and  $T_0 > 0$  is reference temperature [30,34,35]. It is worth mentioning  $n$  is a constant ( $0 \leq n \leq 1$ ). The case  $n=0$  implies  $N=0$  at the sheet and is denotes to the condition of no slip. It symbolizes a flow of concentrated particles in which the wall-bound microelements are incapable of rotating [19,20]. The term "strong

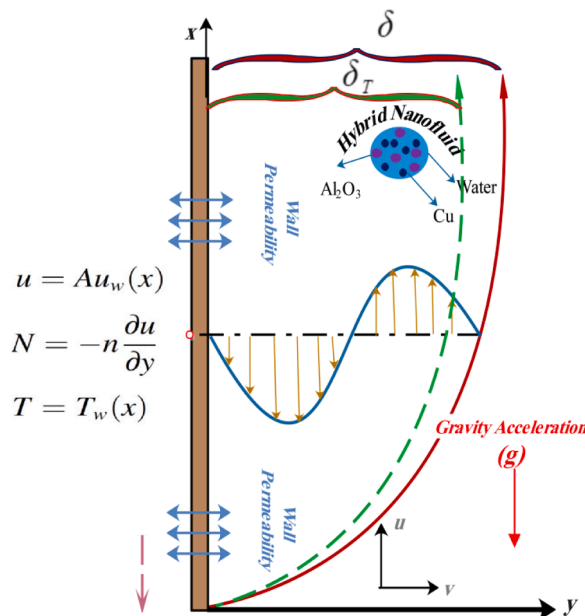


Fig. 1. The schematic, coordinate system, solid-particles, and controlling conditions.

concentration of microelements” also applies to this situation. The stress tensor’s anti-symmetric portion vanishes in the situation  $n=0.5$  [23,30,34]. However, the flow modeling of turbulent uses the scenario  $n=1$  proposed by Peddieson [36]. We have made use of the Tiwari-Das [27] formulation, a single-phase nanofluid. Using this method, we transform the new form of the controlling PDEs (1)-(4), as given in Table 1, into the equal thermophysical characteristics of the binary nanofluid.

It should be noted here that in Table 1, the subscripts  $f, 1, 2$  indicate the quantities of the base liquid,  $Al_2O_3$  solid-particles and  $Cu$  solid-particles, respectively. Table 2 shows the thermophysical features of the base liquid and solid-particles.

For the dynamic viscosity, thermal conductivity, density, thermal expansion capacity, heat capacity, electrical conductivity and characteristics that are specified for  $Al_2O_3$ - $Cu$ /water binary solid-particles; we can present our mass-based formulation model according to Fig. 2. In this model there are 5 equations and 8 unknown, (i.e.  $\phi_1, \phi_2, \phi, m_1, m_2, m_f, \rho_s$  and  $(Cp)_s$  versus the  $(Cp)_1, (Cp)_2, \rho_1, \rho_2$  and  $\rho_f$ ). In our special case  $\rho_s$  and  $(Cp)_s$  is omitted and just three known with three equations can be solved carefully.

Therefore firstly we should obtain masses of solid-particles and base liquid (i.e.  $m_1, m_2$  and  $m_f$ ). Now, we suppose that the velocity vectors ( $u$  and  $v$ ), component of microrotation in x-y plain (N). Consequently, the similarity transformations for the current problem are [4,30,34-37,43]

$$\begin{aligned} \psi &= (\nu_f c)^{1/2} x f(\eta), & N &= c \left(\frac{c}{\nu_f}\right)^{1/2} x g(\eta), & \theta(\eta) &= \frac{T - T_\infty}{T_w - T_\infty}, \\ \eta &= \left(\frac{c}{\nu_f}\right)^{1/2} y, & u &= \frac{\partial \psi}{\partial x} = c x \frac{df}{d\eta}(\eta), & v &= \frac{\partial \psi}{\partial y} = -(c \nu_f)^{1/2} f(\eta). \end{aligned} \tag{6}$$

When the similarity variable is thought of as a linear function of  $y$ , it is significant to note that the relation  $\theta(\eta) = (T - T_\infty) / (T_w - T_\infty)$  can only be valid if  $T$  would be independent of  $x$ . Besides, one can assume  $\partial T / \partial x \gg \partial T / \partial y$  [37]. It implies that we may disregard the temperature’s fluctuation in the x-direction relative to the y-direction, and as a result,  $T$  would be independent of  $x$ .

Although the authors decided to first take into account the 2D equations of boundary layer in general form (See Eqs. (1)–(4)), it is feasible that  $\partial T / \partial x$  would be excluded from energy Eq. (4) concurrently with using the approximations of boundary layer [42]. Continuing the similarity transformation approach, we can convert the initial PDEs (1)-(4) to non-dimensional equations as follows:

$$\gamma_1 (1 + \gamma_2 K) \frac{d^3 f}{d\eta^3} - \left(\frac{df}{d\eta}\right)^2 + f \frac{d^2 f}{d\eta^2} + \gamma_3 K \frac{dg}{d\eta} + Ri \gamma_4 \theta - M \gamma_5 \frac{df}{d\eta} = 0, \tag{7}$$

$$\gamma_1 \left(1 + \frac{\gamma_2 K}{2}\right) \frac{d^2 g}{d\eta^2} + f \frac{dg}{d\eta} - g \frac{df}{d\eta} - \gamma_3 K B \left(2g + \frac{d^2 f}{d\eta^2}\right) = 0, \tag{8}$$

$$\frac{1}{Pr} \frac{\alpha_{hnf}}{\alpha_f} \frac{d^2 \theta}{d\eta^2} + f \frac{d\theta}{d\eta} - \theta \frac{df}{d\eta} + \gamma_6 \delta \left(\theta \frac{dg}{d\eta} - g \frac{d\theta}{d\eta}\right) = 0, \tag{9}$$

$$\begin{aligned} \gamma_1 &= \left(1 - \frac{\frac{m_1 + m_2}{\rho_1 + \rho_2} + \frac{m_f}{\rho_f}}{\frac{m_1 + m_2}{\rho_1 + \rho_2} + \frac{m_f}{\rho_f}}\right)^{-2.5} \left\{1 - \frac{\frac{m_1 + m_2}{\rho_1 + \rho_2} + \frac{m_1 + m_2}{\rho_1 + \rho_2} + \frac{m_f}{\rho_f}}{\frac{m_1 + m_2}{\rho_1 + \rho_2} + \frac{m_f}{\rho_f}}\right\}^{-1}, \\ \gamma_2 &= \left(1 - \frac{\frac{m_1 + m_2}{\rho_1 + \rho_2} + \frac{m_f}{\rho_f}}{\frac{m_1 + m_2}{\rho_1 + \rho_2} + \frac{m_f}{\rho_f}}\right)^{2.5}, \quad \gamma_3 = \left\{1 - \frac{\frac{m_1 + m_2}{\rho_1 + \rho_2} + \frac{m_1 + m_2}{\rho_1 + \rho_2} + \frac{m_f}{\rho_f}}{\frac{m_1 + m_2}{\rho_1 + \rho_2} + \frac{m_f}{\rho_f}}\right\}^{-1}, \end{aligned}$$

**Table 1**  
Properties and relevant formulations for binary nanofluid [2,13,30,37-40].

Property	Relations for binary nanofluid
Viscosity ( $\mu_{hnf}$ )	$\frac{\mu_f}{(1 - \phi)^{2.5}}$
Density ( $\rho_{hnf}$ )	$\phi_1 \rho_1 + \phi_2 \rho_2 + (1 - \phi) \rho_f$ $(1 - \phi) (\rho_f) + \phi (\rho_s)$
Heat capacity ( $\rho C_p$ ) <sub>hnf</sub>	$\phi_1 (\rho C_p)_1 + \phi_2 (\rho C_p)_2 + (1 - \phi) (\rho C_p)_f$
Thermal conductivity ( $k_{hnf}$ )	$\frac{(k_{hp} + 2k_f) - 2\phi(k_f - k_{hp})}{(k_{hp} + 2k_f) + \phi(k_f - k_{hp})} \times (k_f), \quad k_{hp} = \frac{\phi_1 k_1 + \phi_2 k_2}{\phi_1 + \phi_2}$
Thermal diffusivity ( $\alpha_{hnf}$ )	$\frac{k_{hnf}}{(\rho C_p)_{hnf}}$
Thermal expansion capacity ( $\rho \beta$ ) <sub>hnf</sub>	$\phi_1 (\rho \beta)_1 + \phi_2 (\rho \beta)_2 + (1 - \phi) (\rho \beta)_f$
Electrical conductivity ( $\alpha_{hnf}$ )	$\frac{(\sigma_{nf} + 2\sigma_f) - 2\phi(\sigma_f - \sigma_{nf})}{(\sigma_{nf} + 2\sigma_f) + \phi(\sigma_f - \sigma_{nf})} \times (\sigma_f), \quad \sigma_{nf} = \frac{\phi_1 \sigma_1 + \phi_2 \sigma_2}{\phi_1 + \phi_2}$

**Table 2**  
Thermophysical features of base liquid and solid-particles [10,11,30,40-44]

Property	Fluid phase ( $H_2O$ )	$Al_2O_3$	Cu
$\rho(Kg/m^3)$	997.1	3970	8933
$C_p(J/KgK)$	4179	765	385
$k(W/mK)$	0.613	40	401
Particle size (nanometer)	–	13	5-25
$\sigma(\Omega/m)^{-1}$	0.05	$3.69 \times 10^7$	$5.96 \times 10^7$
$\beta \times 10^{-5} (1/K)$	21	0.85	1.67

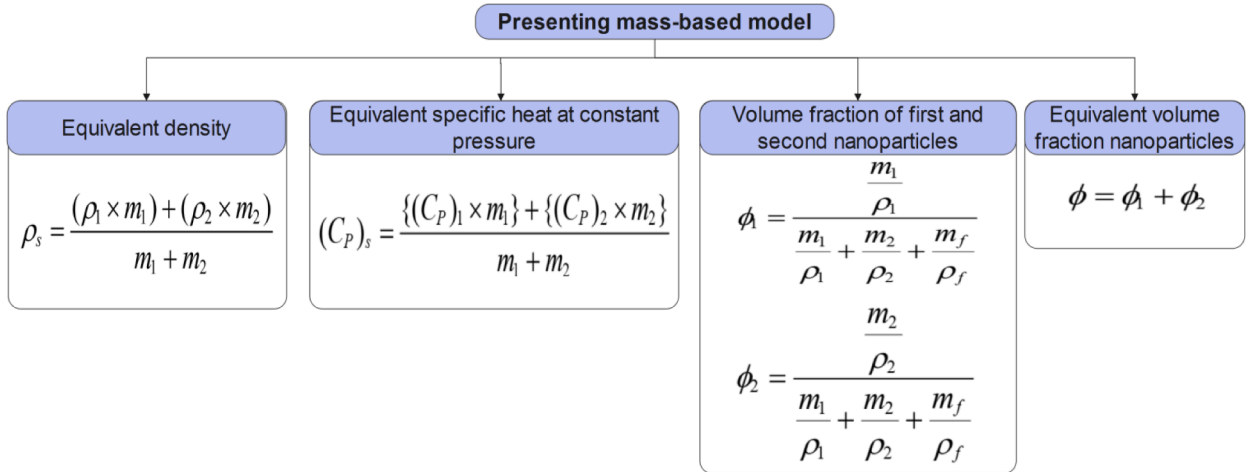


**Fig. 2.** Formulation of new model for binary nanofluid [3,4,29].

$$\gamma_4 = \gamma_3 \left\{ 1 - \frac{\frac{m_1}{\rho_1} + \frac{m_2}{\rho_2}}{\frac{m_1}{\rho_1} + \frac{m_2}{\rho_2} + \frac{m_f}{\rho_f}} + \frac{\rho_1 \beta_1}{\rho_f \beta_f} \left( \frac{\frac{m_1}{\rho_1}}{\frac{m_1}{\rho_1} + \frac{m_2}{\rho_2} + \frac{m_f}{\rho_f}} \right) + \frac{\rho_2 \beta_2}{\rho_f \beta_f} \left( \frac{\frac{m_2}{\rho_2}}{\frac{m_1}{\rho_1} + \frac{m_2}{\rho_2} + \frac{m_f}{\rho_f}} \right) \right\},$$

$$\gamma_5 = \gamma_3 \left( \frac{\frac{\frac{m_1 \sigma_1 + m_2 \sigma_2}{\rho_1 + \rho_2}}{\frac{m_1}{\rho_1} + \frac{m_2}{\rho_2}} + 2\sigma_f - 2 \left( \frac{\frac{m_1 + m_2}{\rho_1 + \rho_2} \right) \left( \sigma_f - \frac{\frac{m_1 \sigma_1 + m_2 \sigma_2}{\rho_1 + \rho_2}}{\frac{m_1}{\rho_1} + \frac{m_2}{\rho_2}} \right)}{\frac{\frac{m_1 \sigma_1 + m_2 \sigma_2}{\rho_1 + \rho_2}}{\frac{m_1}{\rho_1} + \frac{m_2}{\rho_2}} + 2\sigma_f + \left( \frac{\frac{m_1 + m_2}{\rho_1 + \rho_2} \right) \left( \sigma_f - \frac{\frac{m_1 \sigma_1 + m_2 \sigma_2}{\rho_1 + \rho_2}}{\frac{m_1}{\rho_1} + \frac{m_2}{\rho_2}} \right)} \right),$$

$$\gamma_6 = \left\{ \left( 1 - \left( \frac{\frac{m_1}{\rho_1} + \frac{m_2}{\rho_2}}{\frac{m_1}{\rho_1} + \frac{m_2}{\rho_2} + \frac{m_f}{\rho_f}} \right) \right) + \left( \frac{\rho_1 C_{p1}}{\rho_f C_{pf}} \left( \frac{\frac{m_1}{\rho_1}}{\frac{m_1}{\rho_1} + \frac{m_2}{\rho_2} + \frac{m_f}{\rho_f}} \right) + \frac{\rho_2 C_{p2}}{\rho_f C_{pf}} \left( \frac{\frac{m_2}{\rho_2}}{\frac{m_1}{\rho_1} + \frac{m_2}{\rho_2} + \frac{m_f}{\rho_f}} \right) \right) \right\}^{-1}.$$

and boundary conditions are

$$f(0) = S, \quad \frac{df}{d\eta}(0) = A, \quad g(0) = \frac{1}{2} \frac{d^2 f}{d\eta^2}(0), \quad \theta(0) = 1, \quad \text{at} \quad \eta = 0, \tag{10}$$

$$\frac{df}{d\eta}(\infty) = 0, \quad g(\infty) = 0, \quad \theta(\infty) = 0, \quad \text{at} \quad \eta \rightarrow \infty.$$

In above relations, the controlling parameters are the magnetic parameter ( $M$ ) the suction parameter ( $S$ ), the Prandtl number ( $Pr$ ) the Richardson number ( $Rr$ ), the micropolar heat conduction parameter ( $\delta$ ), the shrinking parameter ( $A$ ) and the microinertia parameter ( $B$ ). The component of microrotation is considered,  $n = 1/2$  because the applied conditions of micropolar binary solid-particles are similar to [30]:

$$\begin{aligned}
 S &= \frac{-v_w}{(cv_f)^{1/2}}, & M &= \frac{\sigma B_0^2}{\rho_f c}, & Pr &= \frac{v_f(\rho C_p)_f}{k_f}, \\
 Ri &= \frac{g(\rho\beta)_f(T_w - T_\infty)}{c^2}, & \delta &= \frac{cN^*}{v_f(\rho C)_f}, & B &= \frac{v_f}{(jc)}, & K &= \frac{\kappa}{\eta_f}.
 \end{aligned}
 \tag{11}$$

Here  $S < 0$  denotes the injection case and  $S > 0$  indicates the suction on wall Besides, the Nusselt number and the skin also defines according to the following relations[19,22,31,32]:

$$C_f = \frac{(\mu_{hnf} + \kappa) \left(\frac{\partial u}{\partial y}\right)_{y=0} + (\kappa N)_{y=0}}{\rho_f U_w^2}, \quad Nu_x = \frac{-xk_{hnf} \left(\frac{\partial T}{\partial y}\right)_{y=0}}{k_f(T_w - T_\infty)}.
 \tag{12}$$

with non-dimensional forms as

$$\begin{aligned}
 [Re_x]^{\frac{1}{2}} C_f &= \left\{ \left( 1 - \frac{\frac{m_1}{\rho_1} + \frac{m_2}{\rho_2}}{\frac{m_1}{\rho_1} + \frac{m_2}{\rho_2} + \frac{m_f}{\rho_f}} \right)^{-2.5} + K \right\} \frac{d^2 f}{d\eta^2}(0) + Kg(0), \\
 [Re_x]^{-\frac{1}{2}} Nu_x &= \frac{k_{hnf}}{k_f} \frac{d\theta}{d\eta}(0),
 \end{aligned}
 \tag{13}$$

Meanwhile,  $Re_x = U_w x / v_f$  is the local Reynold’s number, and  $K_{hnf}$  was defined in Table 1.

### 3. Computational algorithm and comparisons

Using the MATLAB (bvp4c function), the controlling Eqs. (7)-(9) were numerically worked out for certain amounts of the emerging parameters  $m_1, m_2, m_f, K, A, Ri, M, Pr, S, \delta$  and  $B$ . We must recast the BVPs as set of first-order ODEs in order to use the bvp4c function. The bvp4c function necessitates a preliminary estimate on the intended outcome for the Eqs. (7)-(9). The estimate should meet the boundary requirements and show how the answer behaves. The bvp4c technique will converge to the answer even for bad estimates; therefore coming up with an initial guess for the solution is not difficult. We begin with a set of parameter amounts for which the issue may be resolved quickly. Then, with just minor changes to the settings, we solve the issue using the acquired answer as our first guess. Until the parameters are set to the appropriate amounts, this is repeated. This method is referred to as continuation. (see Shampine et al. [45]). In this procedure we consider:

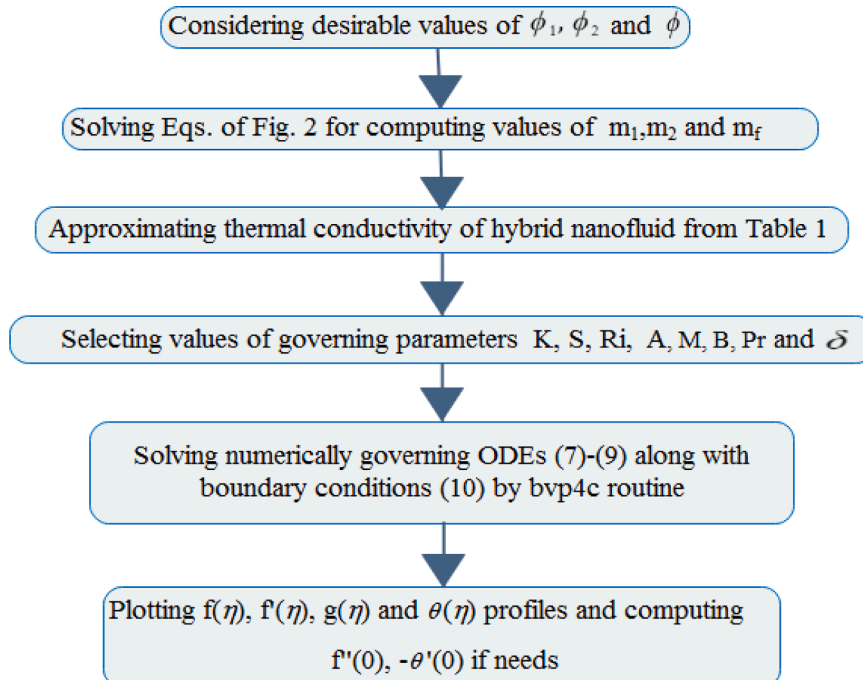


Fig. 3. Flowchart of present computational algorithm.

**Table 3**  
Comparing engineering quantities for pure thermomicroplar fluid in fraction-based model and mass-based model.

<i>K</i>	<i>Ri</i>	<i>A</i>	<i>M</i>	<i>S</i>	$\delta$	<i>Pr</i>	<i>B</i>	$\phi_1$	$\phi_2$	Fraction-based model (Nepal Chandra Roy [30])			Mass-based model (Present)				
										$f''(0)$	$-g(0)$	$-\theta'(0)$	$m_1$	$m_2$	$f''(0)$	$-g(0)$	$-\theta'(0)$
0.25	1	-0.5	0.2	3.2	1	6.2	1	0	0	1.41363	-1.901	23.046	0	0	1.4136	-1.901	23.046
0.1								0	0	1.51781	-2.19203	23.24508	0	0	1.517814	-2.19203	23.24508
0								0	0	1.59592	-2.42401	23.38964	0	0	1.59592	-2.42401	23.38964
0.25	5							0	0	1.570188	-2.125702	23.441464	0	0	1.570188	-2.1257	23.44146
0.25	10							0	0	1.7592205	-2.397433	23.922047	0	0	1.759221	-2.39743	23.92205
0.25	1	-1						0	0	2.604383	-3.257496	26.011273	0	0	2.604383	-3.2575	26.01127
0.25	1	-1	0.1					0	0	2.5651106	-3.201502	25.907308	0	0	2.565111	-3.2015	25.90731
0.25	1	-1	0					0	0	2.5242522	-3.143286	25.799265	0	0	2.524252	-3.14329	25.79927
0.25	1	-1	0.2	2				0	0	1.2547304	-0.661125	14.959751	0	0	1.25473	-0.66113	14.95975
0.25	1	-1	0.2	0				0	0	1.8620878	0.1798077	-11.81502	0	0	1.862088	-0.17981	-11.815
0.25	1	-1	0.2	3.2	0			0	0	2.6164136	-3.274099	19.267714	0	0	2.616414	-3.2741	19.26771
0.25	1	-1	0.2	3.2	1	3		0	0	2.6534766	-3.325912	11.676391	0	0	2.653477	-3.32591	11.67639

**Table 4**  
Comparing engineering quantities for thermomicropolar nanofluid between fraction-based model and mass-based model.

$K$	$Ri$	$A$	$M$	$S$	$\delta$	$Pr$	$B$	$\phi_1$	$\phi_2$	Fraction-based model (Nepal Chandra Roy [30])			$m_1$	$m_2$	Mass-based model (Present)		
										$f''(0)$	$-g(0)$	$-\theta'(0)$			$f''(0)$	$-g(0)$	$-\theta'(0)$
0.25	1	-1	0.2	3.2	1	6.2	1	0.05	0	2.675641	-3.440084	22.236736	21	0	2.675712	-3.44026	22.22963
								0.1	0	2.6754367	-3.436964	18.959404	45	0	2.674381	-3.43411	18.86541
								0	0.05	3.2986529	-5.289321	23.185715	0	47	3.296857	-5.28344	23.19477
								0	0.1	3.7800381	-6.980679	20.187021	0	99.5	3.779736	-6.97954	20.18936

**Table 5**

Comparing engineering quantities for thermomicro-polar binary nanofluid between fraction-based model and mass-based model.

$K$	$Ri$	$A$	$M$	$S$	$\delta$	$Pr$	$B$	$\phi_1$	$\phi_2$	Fraction-based model (Nepal Chandra Roy [30])			$m_1$	$m_2$	Mass-based model (Present)		
										$f''(0)$	$-g(0)$	$-\theta'(0)$			$f''(0)$	$-g(0)$	$-\theta'(0)$
0.25	1	-1	0.2	3.2	1	6.2	1	0.05	0.1	3.5805838	-6.248522	16.858236	23.4	105.4	3.580796	-6.24928	16.86057
								0.1	0.1	3.3351004	-5.404413	14.075583	49.8	112	3.334822	-5.4035	14.07267
								0.1	0.05	3.0954516	-4.638933	16.417311	46.8	52.7	3.095731	-4.6398	16.4217

$$f'' = y(1), \quad f' = y(2), \quad f = y(3), \quad g' = y(4), \quad g = y(5), \quad (14)$$

$$\theta' = y(6) \quad \text{and} \quad \theta = y(7).$$

Therefore, we can write:

$$\frac{d(y(1))}{d\eta} = \frac{-y(3).y(1) + y(1)^2 - K.\gamma_3.y(4) - Ri.\gamma_4.y(7) + \gamma_5.M.y(2)}{\gamma_1(1 + K.\gamma_2)}, \quad \frac{d(y(2))}{d\eta}$$

$$= y(1), \quad \frac{d(y(3))}{d\eta} = y(2), \quad \frac{d(y(4))}{d\eta} = \frac{-y(3).y(4) + y(2).y(5) + K.\gamma_3.B.(2y(5) + y(1))}{\gamma_1(1 + K.\gamma_2/2)}, \quad \frac{d(y(5))}{d\eta} = y(4), \quad (15)$$

$$\frac{d(y(6))}{d\eta} = \frac{-y(3).y(6) + y(2).y(7) - \gamma_6.\delta.(y(4).y(7) - y(5).y(6))}{\frac{\alpha_{mf}}{Pr.\alpha_f}}, \quad \frac{d(y(7))}{d\eta} = y(6).$$

In addition to these modified boundary conditions:

$$ya(3) = S, \quad ya(2) = A, \quad ya(5) = -0.5ya(1), \quad ya(7) = 1, \quad (16)$$

$$yb(2) \rightarrow 0, \quad yb(5) \rightarrow 0, \quad yb(7) \rightarrow 0.$$

In which [ya ,yb] means [0 , η∞] in MATLAB package and shows two-point boundary conditions that should be obtained later. These preliminary estimates should meet the boundary criteria. Finally, a summary of our computational approach is shown in Fig. 3.

To validate present computational method, the amount of the shear stress, the microrotation gradient, and heat transfer for three cases (i.e. pure thermomicro-polar fluid, thermomicro-polar nanofluid and thermomicro-polar binary nanofluid) are compared with already reported achievements. These comparisons are shown in Tables 3, 4, and 5, respectively. In Table 3 (for pure thermomicro-polar fluid) different characteristics are compared in fraction-based model and mass-based model. Comparison of engineering interests for different fractions of one type of particle in absence of other has been tabulated in Table 4. At last Table 5 shows these comparisons for thermomicro-polar binary nanofluid. In Tables 4 and 5 except ϕ<sub>1</sub> and ϕ<sub>2</sub>, other characteristics has been taken constant. Thus, it can be said that the created approach may be utilized to investigate the heat and fluid flow of the current situation with a high degree of certainty.

#### 4. Results and discussion

In this division, the attribute of thermomicro-polar binary nanofluid flow transiting over moving and permeable, under influence of steady magnetic ground, has been scrutinized. It is worthwhile to notice that in Section 4.1, we have focused on engineering interests (the shear stress aspect f''(0), the microrotation gradient aspect g'(0), and the heat transfer aspect -θ'(0)) for various amounts of controlling parameters such as the first solid-particle mass m<sub>1</sub>, second solid-particle mass m<sub>2</sub>, mass of base liquid m<sub>f</sub>, material parameter K, shrinking parameter A, Richardson number Ri, magnetic ground parameter M, Prandtl number Pr, suction parameter S, micropolar heat conduction parameter δ, and the microinertia parameter B. Also in the Section 4.2, the temperature aspect -θ(0), velocity aspect f'(0), and the angular velocity aspect g(0), are plotted and analyzed.

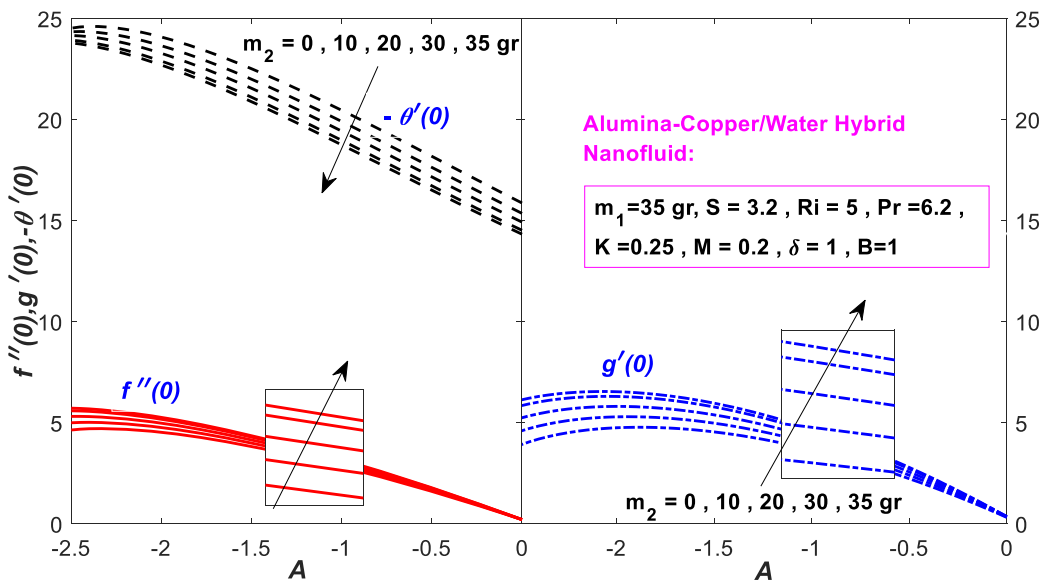


Fig. 4. f''(0), g'(0), and -θ'(0) for various amounts of m<sub>2</sub> with m<sub>1</sub> = 35gr, S = 3.2, Ri = 5, Pr = 6.2, K = 0.25, M = 0.2, δ = 1, B = 1.

4.1. Quantities of interest in engineering concepts

The changes of the heat transfer, shear stress and microrotation gradient as a function of shrinking A, with different amounts of  $m_2$  (copper solid-particle mass), are shown in Fig. 4. It is found that heat transfer, shear stress and microrotation gradient firstly augment and then reduce with the enhancement of the shrinking parameter A. For increasing amount of  $m_2$ , the shear stress and microrotation gradient increase but heat transfer significantly decreases. According to former research (Khan et al [34]), the influences of two equal solid volume fractions of different solid-particles and the stretching/shrinking parameter A on the rate of heat transfer, the microrotation gradient, and shear stress produced outcomes similar to those of the current study.

The suction parameter influences on heat transfer, shear stress and the microrotation gradient, is exhibited in Fig. 5. The graphical achievements illustrate that an augmentation in the suction parameter significantly enhances the heat transfer, shear stress and the microrotation gradient, but it can be declared that the influences of S on  $f''(0)$  is less than the  $-\theta'(0)$  and  $g'(0)$ . In Fig. 5, first we can see a growth, then a decline on the graphs. The increase in suction causes a thinner hydrodynamics boundary layer. This issue means a high-velocity gradient on the wall that enhances skin friction. Although it should be noted that suction expedites to transition to a turbulent regime and can delay separation in the boundary layer in the curved surfaces. Usually, an optimum suction is detectable for researchers to favorable goals. Moreover, Fig. 5 demonstrates a considerable increase in heat transfer with suction which is a reasonable result and also reported by former researchers.

The heat transfer, shear stress and microrotation gradient as a function of shrinking parameter are investigated by the influences of the magnetic ground parameter M, in Fig. 6. With the increase of the magnetic ground parameter, there can be seen a considerable enhancement in them. For  $A \geq -1.5$ , the magnetic ground has a very weak influence on the heat transfer, shear stress and microrotation gradient. These phenomena can be significant in industries such as rolling steel sheets, which magnetic fields used widely there.

Fig. 7 illustrates how the material parameter K affects the microrotation gradient, shear stress, and heat transfer. Heat transfer, shear stress, and microrotation gradient all significantly decrease with rising K amount [46]. Additionally, the outcome showed that a rise in the material parameter was seen to reduce the local Nusselt number of the micropolar binary nanofluid. The influence of augmenting K in  $g'(0)$  is noticeably greater than two others.

The influences of the Richardson's number Ri on the heat transfer, shear stress and gradient of microrotation are demonstrated in Fig. 8. It is observed here that the effect of Ri on shear stress, gradient of microrotation and heat transfer is poor, however, they also increase in the same direction as Ri. Mahmoudi et al. [47] declared that at higher Re and Ri, increasing of nanoparticles on heat transfer performance are more effective than two others.

The varying of the heat transfer, shear stress and microrotation gradient as function of shrinking parameter, for some quantities of micropolar heat conduction parameter  $\delta$  are illustrated in Fig. 9. A negligible reduction in the shear stress and microrotation gradient can be observed, when the amounts of  $\delta$  are increased. Nevertheless, with the change of the amounts of  $\delta$ , the heat transfer increases drastically.

4.2. Profiles of interest in physical concepts

In this section, the influences of controlling parameters on the velocity,  $f(\eta)$ , angular velocity,  $g(\eta)$ , and temperature,  $\theta(\eta)$ , are investigated to analyze the boundary layer behavior of thermomicropolar binary nanofluid. In Fig. 10, the influences of the mass of

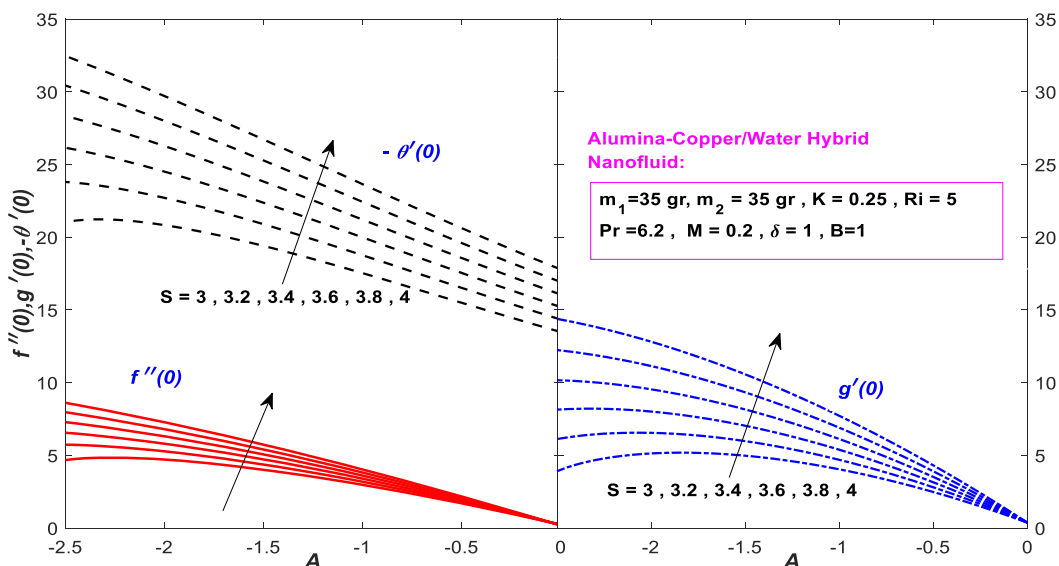


Fig. 5.  $f''(0)$ ,  $g'(0)$ , and  $-\theta'(0)$  for various amounts of S with  $m_1 = 35\text{gr}$ ,  $m_2 = 35\text{gr}$ ,  $Ri = 5$ ,  $Pr = 6.2$ ,  $K = 0.25$ ,  $M = 0.2$ ,  $\delta = 1$ ,  $B = 1$ .

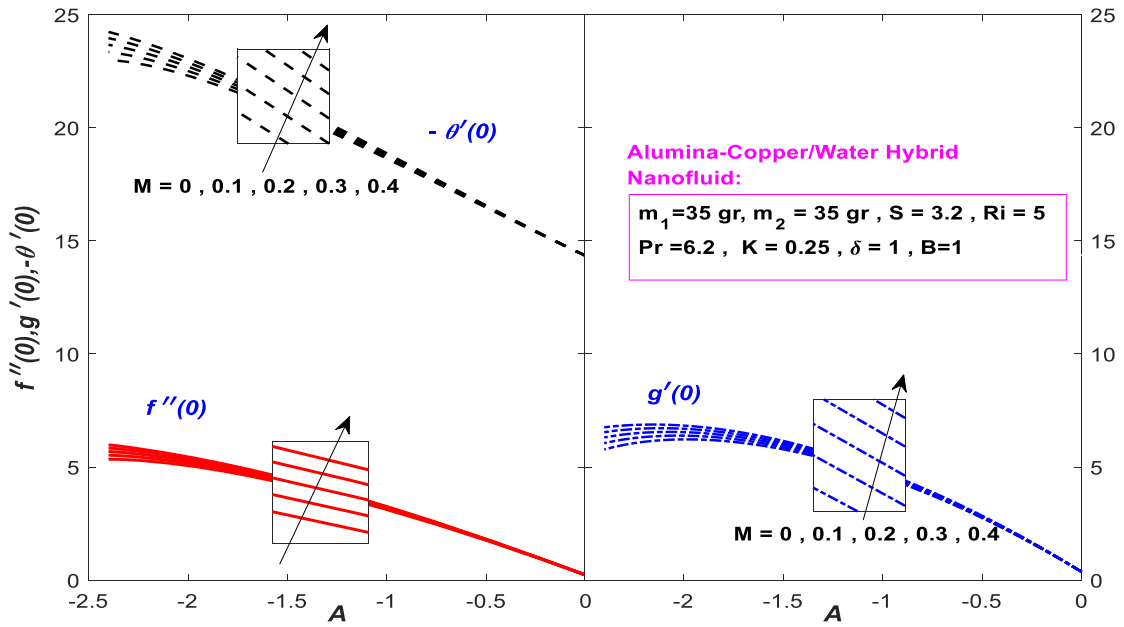


Fig. 6.  $f''(0)$ ,  $g'(0)$ , and  $-\theta'(0)$  for various amounts of  $M$  with  $m_1 = 35gr$ ,  $m_2 = 35gr$ ,  $Ri = 5$ ,  $Pr = 6.2$ ,  $K = 0.25$ ,  $S = 3.2$ ,  $\delta = 1$ ,  $B = 1$ .

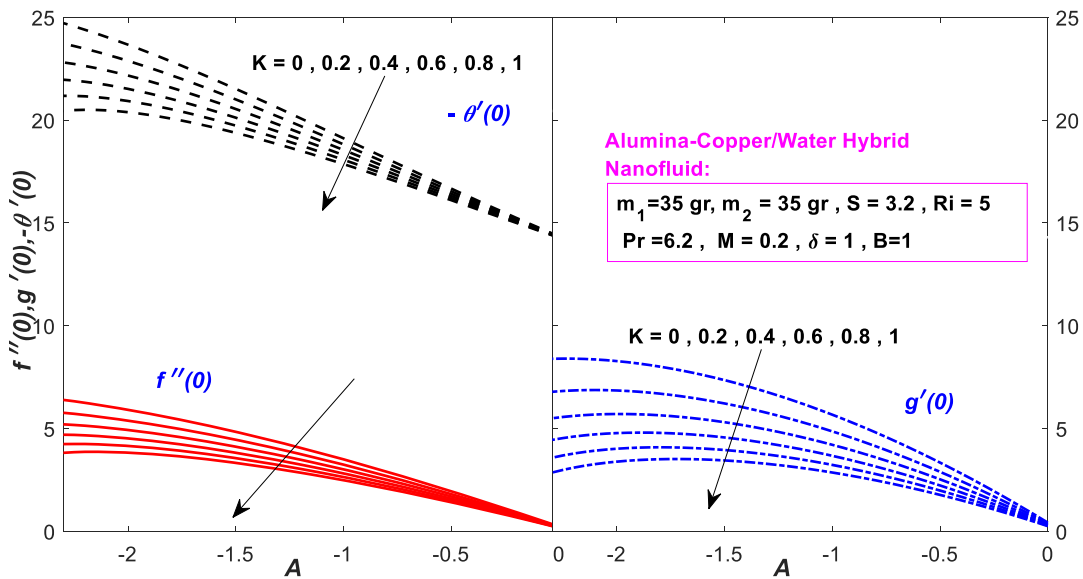


Fig. 7.  $f''(0)$ ,  $g'(0)$ , and  $-\theta'(0)$  for various amounts of  $K$  with  $m_1 = 35gr$ ,  $m_2 = 35gr$ ,  $Ri = 5$ ,  $Pr = 6.2$ ,  $K = 0.25$ ,  $S = 3.2$ ,  $\delta = 1$ ,  $B = 1$ .

copper solid-particles,  $m_2$ , on the velocity, angular velocity, and temperature, versus similarity variable,  $\eta$ , are depicted. It has resulted that due to the increase of  $m_2$ , the temperature and velocity are found to enhance. But in  $g(\eta)$  diagrams close to  $\eta=0.5$ , a turning point is observed so that the behavior of the angular velocities before it decreases and vice versa after it. Adding Cu nanoparticles have smooth effects on all profiles of  $f'(\eta)$ ,  $g(\eta)$  and  $\theta(\eta)$ ; as well such behavior can be also seen in the investigation by Khan et al. [34] on three desired distributions. The figures demonstrate that the far field boundary requirements (10), which are required to validate the numerical findings, are asymptotically met. Due to the influence of the second solid-particle Cu, the energy is physically lost as heat, raising the temperature in the boundary layer. Similarly, Waini et al. [43] have reported that with increasing solid-particle fraction, the velocity promotes too.

Behaviors of velocities and thermal boundary layers with changes of shrinking parameter  $A$  are demonstrated in Fig. 11. Drastic descending can be seen on velocity and angular velocity (with no inflection point) but the decreasing of temperature's profile is not so much. Similarly, Soid et al. [47] have depicted that the velocity decreases with augmenting the magnitude of  $A$ . The  $\theta(\eta)$  shows positive

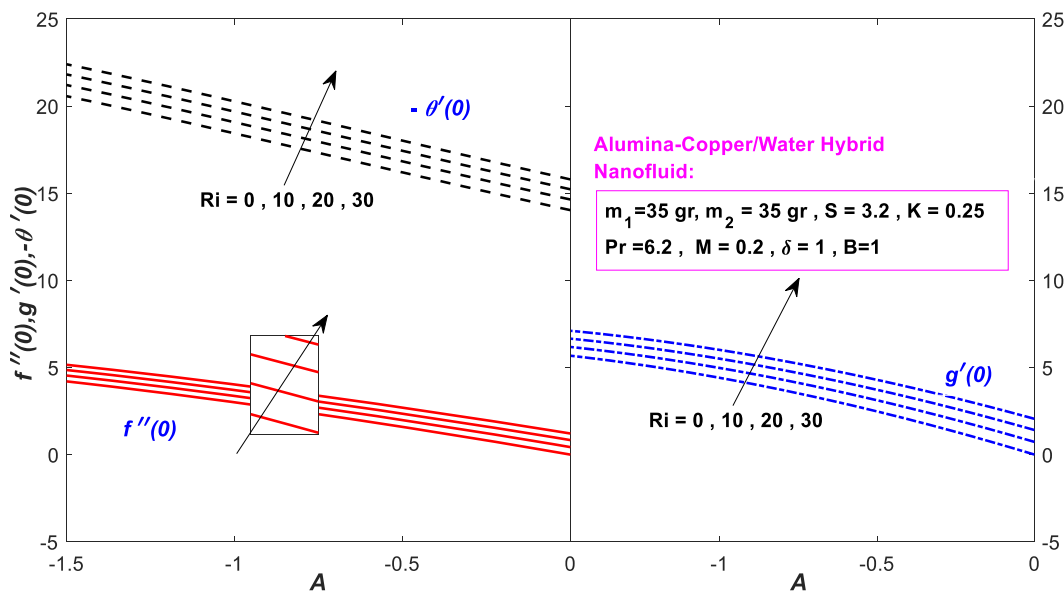


Fig. 8.  $f''(0)$ ,  $g'(0)$ , and  $-\theta'(0)$  for various amounts of  $Ri$  with  $m_1 = 35gr$ ,  $m_2 = 35gr$ ,  $M = 0.2$ ,  $Pr = 6.2$ ,  $K = 0.25$ ,  $S = 3.2$ ,  $\delta = 1$ ,  $B = 1$ .

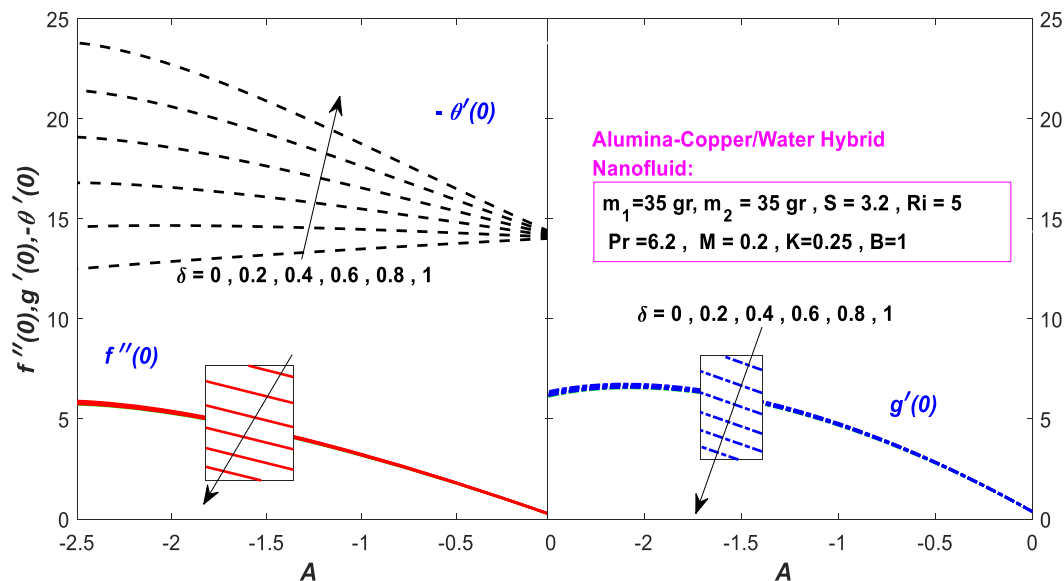


Fig. 9.  $f''(0)$ ,  $g'(0)$ , and  $-\theta'(0)$  for various amounts of  $\delta$  with  $m_1 = 35gr$ ,  $m_2 = 35gr$ ,  $M = 0.2$ ,  $Pr = 6.2$ ,  $K = 0.25$ ,  $S = 3.2$ ,  $Ri = 5$ ,  $B = 1$ .

amounts of gradient at the wall and the profiles reduce rapidly from an amount of one and decrease gently to zero as  $\eta$  enhances. Physically, It demonstrates that first the wall's temperature is higher than fluid and the heat slowly disperses from the wall to the fluid [48]. According to results of Waini et al. [43] the velocity decreases with decreasing of shrinking parameter.

Fig. 12 shows the influences of the suction parameter  $S$  on the velocity, rotation velocity, and temperature. It is clear that when the suction parameter's amounts increase, the velocity profile will accelerate while the temperature profile will decelerate. In other hands, for the angular velocity an inflection point is observed clearly, so before that point the angular velocity descends and after that its profile ascends. In the recent similar investigations, Bhattacharyya et al. [26] have introduced a similar result for angular velocity. According to Mishra et al. [49], the velocity profile rises as the mass suction parameter's amount rises. The profile begins with a negative amount that satisfies the boundary surface requirement and eventually goes asymptotically to zero. It is also significant to note that the velocity and microrotation patterns shown in Fig. 12 are comparable to those shown in the article by Roşca et al. [35] for a number of amounts of the suction parameter  $S$ .

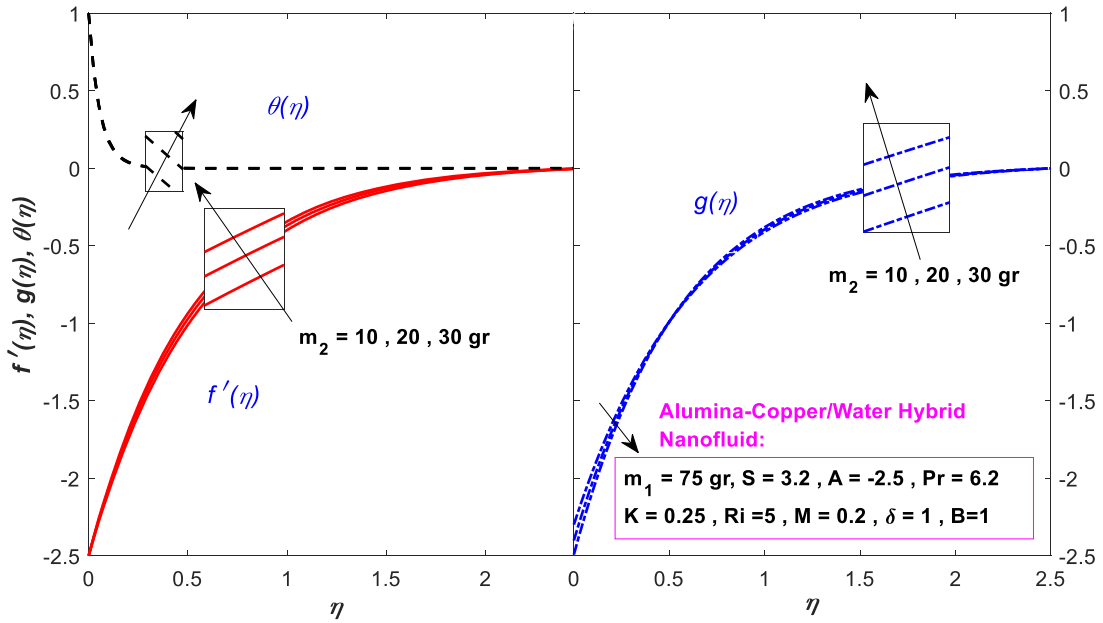


Fig. 10.  $f'(\eta)$ ,  $g(\eta)$ , and  $\theta(\eta)$  for various amounts of  $m_2$  with  $m_1 = 75\text{gr}$ ,  $A = -2.5$ ,  $M = 0.2$ ,  $\text{Pr} = 6.2$ ,  $K = 0.25$ ,  $S = 3.2$ ,  $\text{Ri} = 5$ ,  $\delta = 1$ ,  $B = 1$ .

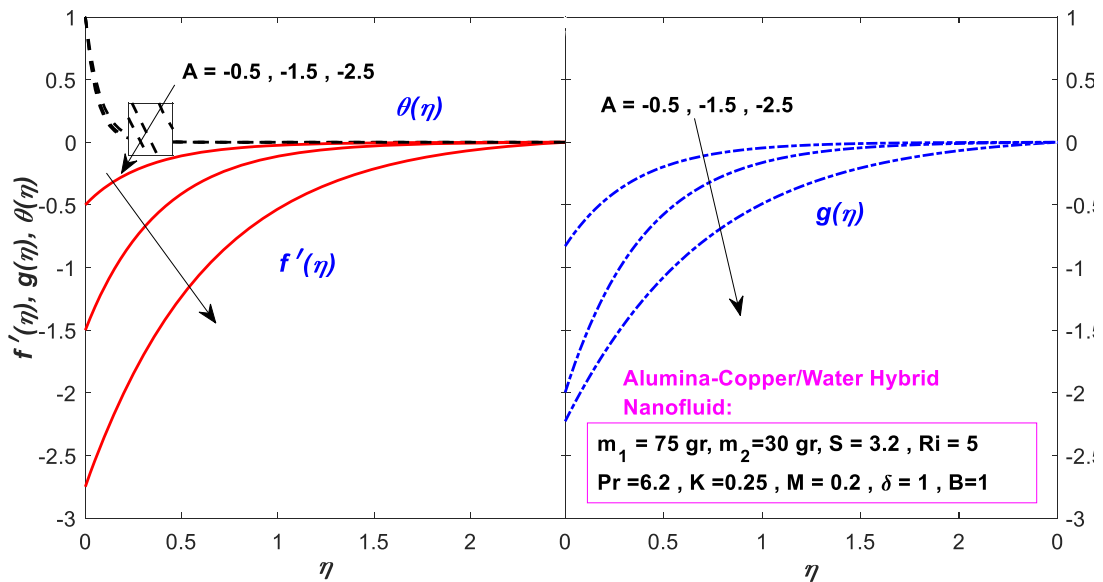


Fig. 11.  $f'(\eta)$ ,  $g(\eta)$ , and  $\theta(\eta)$  for various amounts of  $A$  with  $m_1 = 75\text{gr}$ ,  $m_2 = 30\text{gr}$ ,  $M = 0.2$ ,  $\text{Pr} = 6.2$ ,  $K = 0.25$ ,  $S = 3.2$ ,  $\text{Ri} = 5$ ,  $\delta = 1$ ,  $B = 1$ .

Fig. 13 demonstrates the changes of the velocity, angular velocity, and temperature, versus the similarity variable for the different amounts of magnetic ground parameter  $M$  [50,51]. It is seen that for increasing of  $M$ , the temperature decreases slowly and the velocity augments but negligible increasing of angular velocity happens after an inflection point. Decreasing of angular velocity before inflection point is remarkable. According to Roy et al. [37], when the magnetic ground parameter's amount rises, the binary nanofluid's velocity rises and its temperature falls. Due to the increase in magnetic ground intensity, the momentum and thermal boundary layers thin out a little amount as a result. As in Fig. 6, here we see that the effect of  $M$  is greater at the beginning of the graphs, where we are closest to the wall.

Fig. 14 illustrates how the material parameter  $K$  affects temperature, velocity, and angular velocity. The solutions expose that with the increase of amount of  $K$  the velocity decreases but the temperature enhances. Angular velocity again behaves like as we can see on

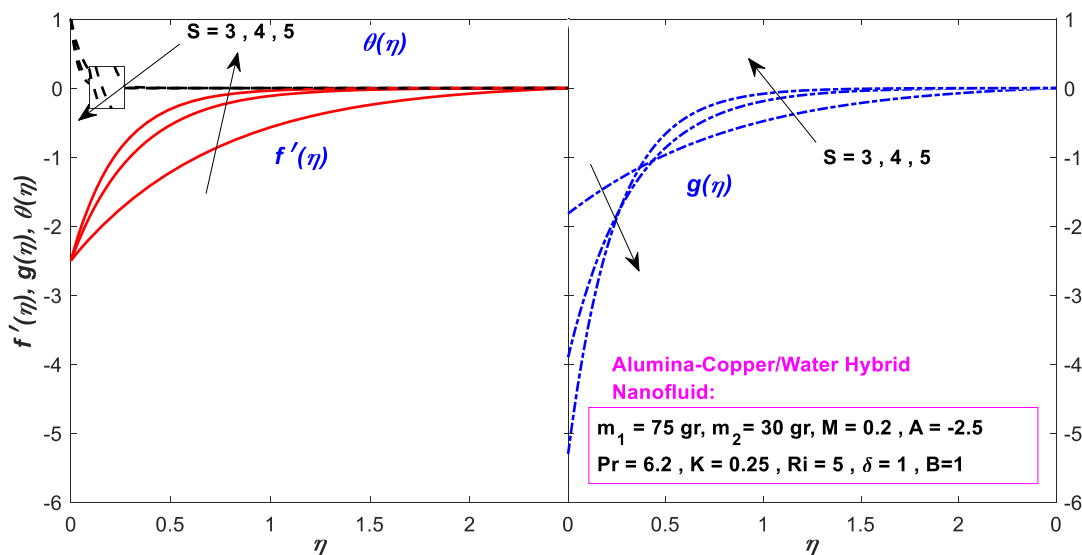


Fig. 12.  $f'(\eta)$ ,  $g(\eta)$ , and  $\theta(\eta)$  for various amounts of  $S$  with  $m_1 = 75\text{gr}$ ,  $m_2 = 30\text{gr}$ ,  $M = 0.2$ ,  $Pr = 6.2$ ,  $K = 0.25$ ,  $A = -2.5$ ,  $Ri = 5$ ,  $\delta = 1$ ,  $B = 1$ .

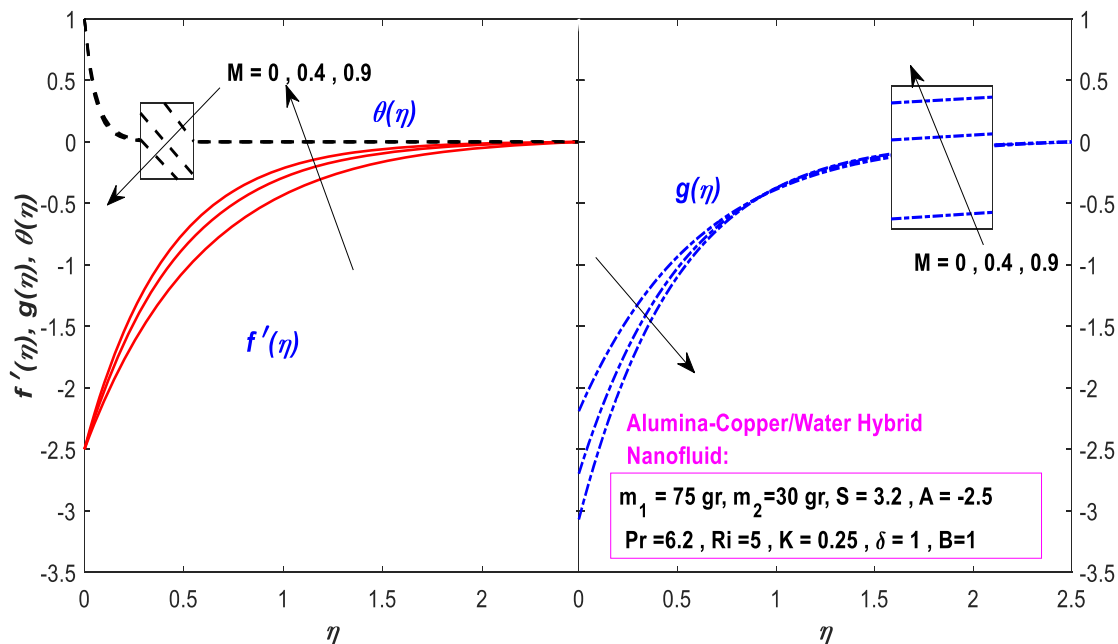


Fig. 13.  $f'(\eta)$ ,  $g(\eta)$ , and  $\theta(\eta)$  for various amounts of  $M$  with  $m_1 = 75\text{gr}$ ,  $m_2 = 30\text{gr}$ ,  $S = 3.2$ ,  $Pr = 6.2$ ,  $K = 0.25$ ,  $A = -2.5$ ,  $Ri = 5$ ,  $\delta = 1$ ,  $B = 1$ .

$M$ ,  $S$ ,  $m_2$  and  $K$ ; while it has an inflection point. It augments before that point and reduces after it. Similar results have obtained for temperature and velocity by Bhattacharyya et al. [26]. According to Mahmood et al. [50], the temperature profile improves as  $K$  rises. It is crucial to note that while the thickness of the thermal boundary layer grows as  $K$  increases, the influence on the surface temperature gradient is quite the reverse [52,53]. It can be shown from the analysis by Khan et al. [54] that the velocity falls off when  $K$  is elevated. The velocity behavior of the material parameter here is the same as in Fig. 7, but the temperature and angular velocity behaviors are different.

Figs. 15 and 16 show how the Richardson's number  $Ri$  affects velocity, angular velocity, and temperature. Although there is a negligible influence of  $Ri$  on the flow characteristics, but a bit decrease can be seen on the temperature and angular velocity while a little augment in velocity is shown. There is not inflection point on angular velocity profile. Similarly, Lund et al. [22] investigated the impact of the Richardson number on the velocity and temperature profiles and resulted in a slight growth in the thermal boundary

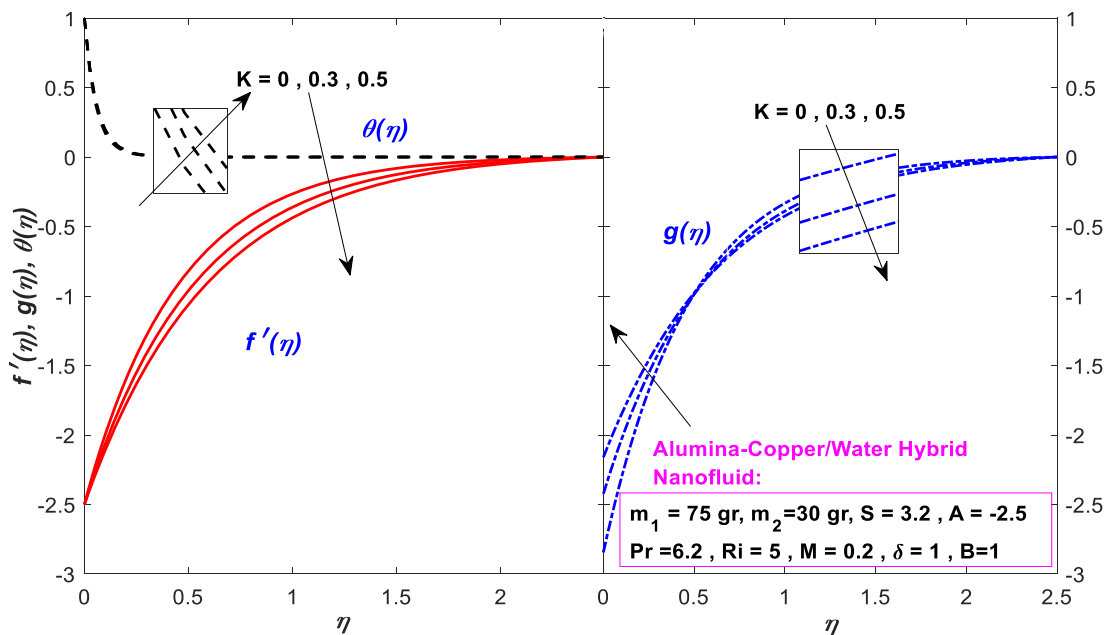


Fig. 14.  $f'(\eta)$ ,  $g(\eta)$ , and  $\theta(\eta)$  for various amounts of  $K$  with  $m_1 = 75\text{gr}$ ,  $m_2 = 30\text{gr}$ ,  $M = 0.2$ ,  $Pr = 6.2$ ,  $S = 3.2$ ,  $A = -2.5$ ,  $Ri = 5$ ,  $\delta = 1$ ,  $B = 1$ .

layer when  $Ri$  is enhanced. Again, as we saw in Fig. 8, the  $Ri$  effect on velocity, angular velocity and temperature profiles is very small.

As it is clear from Fig. 16, the influence of micropolar heat conduction parameter  $\delta$  on the velocity and angular velocity is very weak. Meanwhile, the increasing of  $\delta$  has a little positive influence on growth of angular velocity profile and it has a bit negative influence on velocity. The temperature remarkably decreases with the enhancement of  $\delta$ . In this regards, higher amounts of the micropolar heat conduction parameter can decrease the thickness of thermal boundary layer. In Fig. 9, the additive effect of  $\delta$  on heat transfer was greater than the other cases. Similarly in Fig. 16, increasing  $\delta$  on temperature has a greater effect than velocity and angular velocity.

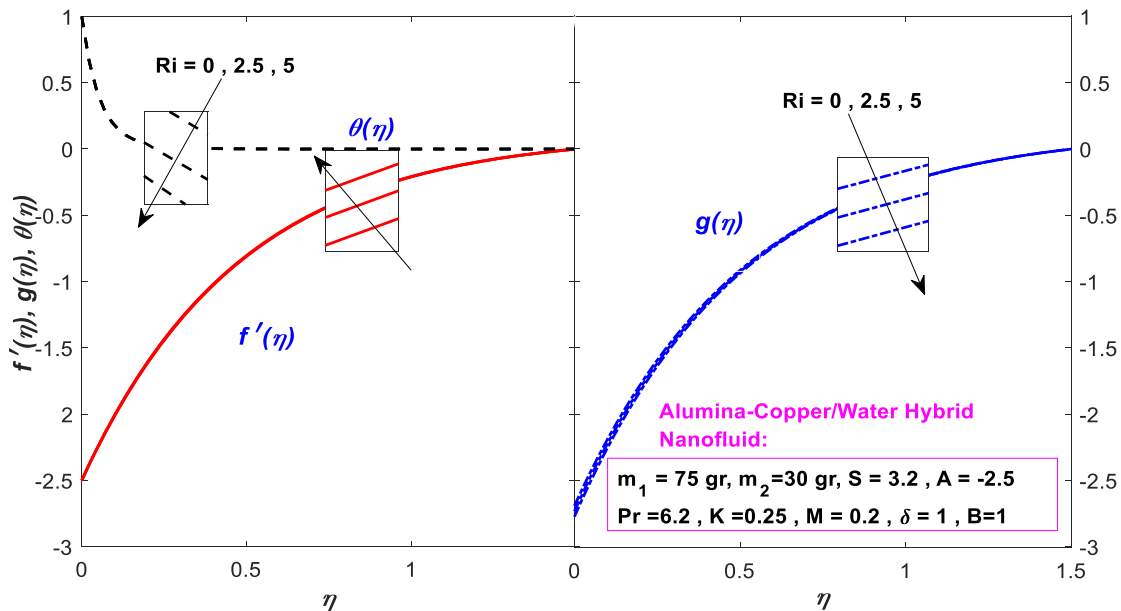


Fig. 15.  $f'(\eta)$ ,  $g(\eta)$ , and  $\theta(\eta)$  for various amounts of  $Ri$  with  $m_1 = 75\text{gr}$ ,  $m_2 = 30\text{gr}$ ,  $M = 0.2$ ,  $Pr = 6.2$ ,  $K = 0.25$ ,  $A = -2.5$ ,  $S = 3.2$ ,  $\delta = 1$ ,  $B = 1$ .

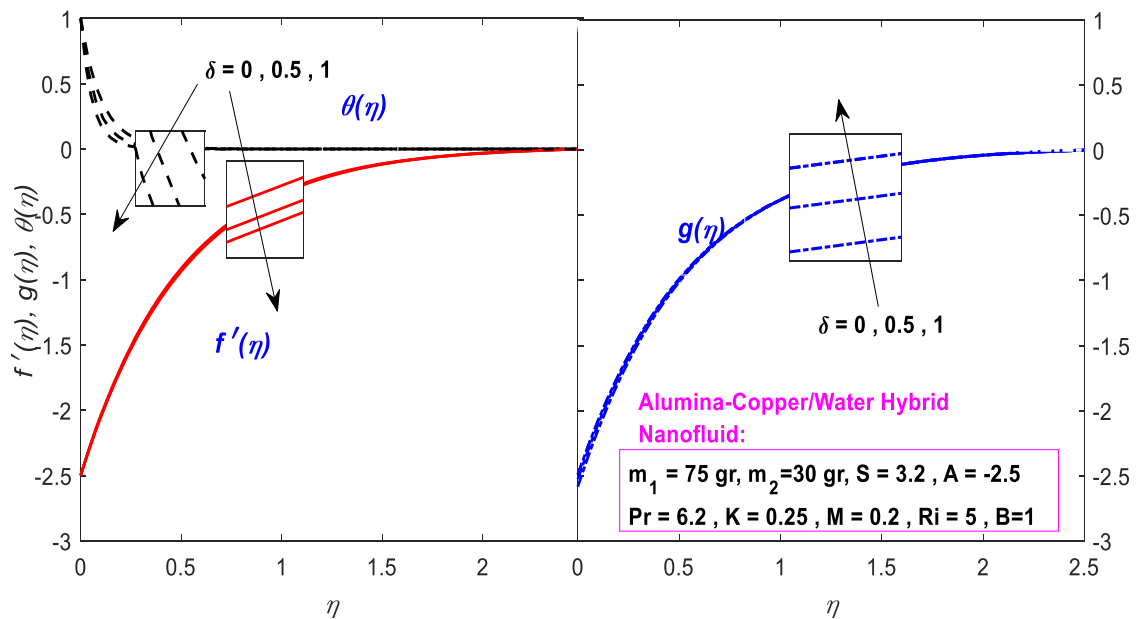


Fig. 16.  $f'(\eta)$ ,  $g(\eta)$ , and  $\theta(\eta)$  for various amounts of  $\delta$  with  $m_1 = 75\text{gr}$ ,  $m_2 = 30\text{gr}$ ,  $M = 0.2$ ,  $\text{Pr} = 6.2$ ,  $S = 3.2$ ,  $K = 0.25$ ,  $A = -2.5$ ,  $Ri = 5$ ,  $B = 1$ .

## 5. Final remarks

In the current work, a steady laminar thermomicro-polar binary nanofluid flow caused by a shrinking sheet with suction and convective boundary conditions in the presence of a transverse magnetic ground was studied using a mass-based model. The approach is based on the single-phase Tiwari-Das binary nanofluid model, which considers base liquid mass and solid-particle mass in instead of first and second solid-particle volume fraction. The dimensional controlling equations of this issue are converted into nonlinear BVPs of ordinary differential equations using similarity variables, and the `bvp4c` function of Matlab is then used to solve them numerically. Comparing the results that have already been published and show high agreement serves as validation. Additionally, the influences of the significant factors on the thermomicro-polar binary nanofluid velocity, angular velocity, temperature distribution, shear stress, microrotation gradient, and heat transfer have been investigated through the tabular and graphical findings. Some remarkable conclusions are described as follows: i) regardless of positive or negative influence, the influences of the increasing of  $m_2$ ,  $S$  and  $K$  are more than  $M$  and  $Ri$  on the shear stress, the microrotation gradient, and the heat transfer. Moreover, the influence of the augmenting of  $\delta$  on heat transfer is drastic; ii) the results demonstrate that the velocity, angular velocity and temperature are impressed, by the augmenting of  $K$ ,  $M$ ,  $m_2$ ,  $\delta$  and  $Ri$ . Besides, the increasing of  $S$  and  $A$  have more influence on velocity and angular velocity than temperature; iii) with its many advantages, such as ease of use and the ability to compute thermophysical parameters of thermomicro-polar binary nanofluids using the masses of both base liquid and solid-particles, the mass-based model may be confidently applied to a variety of theoretical issues.

## Declaration of Competing Interest

The authors declare that they have no known competing financial interests or personal relationships that could have appeared to influence the work reported in this paper.

## Acknowledgments

The authors wish to thank the reviewers for their careful, unbiased and constructive suggestions, which led to this revised manuscript.

## References

- [1] I. Ahmad, H. Zahid, F. Ahmad, M.A.Z. Raja, D. Baleanu, Design of computational intelligent procedure for thermal analysis of porous fin model, *Chin. J. Phys.* 59 (2019) 641–655, <https://doi.org/10.1016/j.cjph.2019.04.015>.
- [2] A. Abdulkadhim, I.M. Abed, N.M. Said, An exhaustive review on natural convection within complex enclosures: influence of various parameters, *Chin. J. Phys.* 74 (2021) 365–388, <https://doi.org/10.1016/j.cjph.2021.10.012>.
- [3] H. Berrehal, S. Dinarvand, I. Khan, Mass-based hybrid nanofluid model for entropy generation analysis of flow upon a convectively-warmed moving wedge, *Chin. J. Phys.* 77 (2022) 2603–2616, <https://doi.org/10.1016/j.cjph.2022.04.017>.

- [4] S.M. Mousavi, M.N. Rostami, M. Yousefi, S. Dinarvand, I. Pop, M.A. Sheremet, Dual solutions for Casson hybrid nanofluid flow due to a stretching/shrinking sheet: a new combination of theoretical and experimental models, *Chin. J. Phys.* 71 (2021) 574–588, <https://doi.org/10.1016/j.cjph.2021.04.004>.
- [5] S. Nasir, A.S. Berrouk, A. Tassaddiq, A. Aamir, N. Akkurt, T. Gul, Impact of entropy analysis and radiation on transportation of MHD advance nanofluid in porous surface using Darcy-Forchheimer model, *Chem. Phys. Lett.* 811 (2023), 140221, <https://doi.org/10.1016/j.cplett.2022.140221>.
- [6] M. Izady, S. Dinarvand, I. Pop, A.J. Chamkha, Flow of aqueous Fe<sub>2</sub>O<sub>3</sub>-CuO hybrid nanofluid over a permeable stretching/shrinking wedge: a development on Falkner-Skan problem, *Chin. J. Phys.* 74 (2021) 406–420, <https://doi.org/10.1016/j.cjph.2021.10.018>.
- [7] H.S. Chahregh, S. & Dinarvand, TiO<sub>2</sub>-Ag/blood hybrid nanofluid flow through an artery with applications of drug delivery and blood circulation in the respiratory system, *Int. J. Numer. Methods Heat Fluid Flow* 30 (11) (2020) 4775–4796, <https://doi.org/10.1108/HFF-10-2019-0732>.
- [8] A. Hussanan, M.Z. Salleh, I. Khan, Sh. Shafie, Convection heat transfer in micropolar nanofluids with oxide nanoparticles in water, kerosene and engine oil, *J. Mol. Liq.* 229 (2017) 482–488, <https://doi.org/10.1016/j.molliq.2016.12.040>.
- [9] S. Dinarvand, M.N. Rostami, Rotating Al<sub>2</sub>O<sub>3</sub>-H<sub>2</sub>O nanofluid flow and heat transfer with internal heating, velocity slip and different shapes of nanoparticles, *Multidiscip. Model. Mater. Struct.* 17 (2) (2020) 401–417, <https://doi.org/10.1108/MMMS-01-2020-0017>.
- [10] N. Abbas, K. Ur Rehman, W. Shatanawi, K. Abodayeh, Mathematical model of temperature-dependent flow of power-law nanofluid over a variable stretching Riga sheet, *Waves Random Complex Media* (2022), <https://doi.org/10.1080/17455030.2022.2111029>. Published online.
- [11] U.S. Mahabaleshwar, Emad H. Aly, T. Anusha, MHD slip flow of a Casson hybrid nanofluid over a stretching/shrinking sheet with thermal radiation, *Chin. J. Phys.* 80 (2022) 74–106, <https://doi.org/10.1016/j.cjph.2022.06.008>.
- [12] S. Dinarvand, M.N. Rostami, I. Pop, A novel hybridity model for TiO<sub>2</sub>-CuO/water hybrid nanofluid flow over a static/moving wedge or corner, *Sci. Rep.* 9 (1) (2019) 1–11, <https://doi.org/10.1038/s41598-019-52720-6>.
- [13] I. Pop, M.Nademi Rostami, S. Dinarvand, Dual similarity solutions because of mixed convective flow of a double-nanoparticles hybrid nanofluid: critical points and stability analysis, *Int. J. Numer. Methods Heat Fluid Flow* 31 (11) (2021) 3319–3342, <https://doi.org/10.1016/j.cjph.2018.06.013>.
- [14] S. Suresh, K. P. Venkataraj, P. Selvakumar, M. Chandrasekar, Synthesis of Al<sub>2</sub>O<sub>3</sub>-Cu/water hybrid nanofluids using two step method and its thermophysical properties, *Colloids Surf. A* 388 (2011) 41–48, <https://doi.org/10.1016/j.colsurfa.2011.08.005>.
- [15] I. Waini, A. Ishak, I. Pop, Hybrid nanofluid flow induced by an exponentially shrinking sheet, *Chin. J. Phys.* 68 (2020) 468–482, <https://doi.org/10.1016/j.cjph.2019.12.015>.
- [16] A.C. Eringen, Theory of micropolar fluids, *J. Math. Mech.* 16 (1966) 1–18, <https://doi.org/10.1512/iumj.1967.16.16001>.
- [17] A.C. Eringen, Theory of thermomicrofluids, *J. Math. Anal. Appl.* 38 (1972) 480–496, [https://doi.org/10.1016/0022-247X\(72\)90106-0](https://doi.org/10.1016/0022-247X(72)90106-0).
- [18] R.S.R. Gorla, Micropolar boundary layer at a stagnation point on a moving wall, *Int. J. Eng. Sci.* 21 (1) (1983) 25–34, [https://doi.org/10.1016/0020-7225\(83\)90036-8](https://doi.org/10.1016/0020-7225(83)90036-8).
- [19] S.K. Jena, M.N. Mathur, Similarity solutions for laminar free convection flow of a thermomicrofluid past a non-isothermal vertical flat plate, *Int. J. Eng. Sci.* 19 (1981) 1431–1439, [https://doi.org/10.1016/0020-7225\(81\)90040-9](https://doi.org/10.1016/0020-7225(81)90040-9).
- [20] S.K. Jena, M.N. Mathur, Free convection in the laminar boundary layer flow of a thermomicrofluid past a vertical plate with suction/injection, *Acta Mech.* 42 (1982) 227–238, <https://doi.org/10.1007/BF01177194>.
- [21] A. Ishak, R. Nazar, I. Pop, Dual solutions in mixed convection boundary layer flow of micropolar fluids, *Commun. Nonlinear Sci. Numer. Simul.* 14 (2009) 1324–1333, <https://doi.org/10.1016/j.cnsns.2008.01.017>.
- [22] L.A. Lund, Z. Omar, I. Khan, Mathematical analysis of magnetohydrodynamic (MHD) flow of micropolar nanofluid under buoyancy effects past a vertical shrinking surface: dual solutions, *Heliyon* 5 (2019), e02432, <https://doi.org/10.1016/j.heliyon.2019.e02432>.
- [23] N. Abbas, W. Shatanawi, Theoretical survey of time-dependent micropolar nanofluid flow over a linear curved stretching surface, *Symmetry* 14 (2022) 1629, <https://doi.org/10.3390/sym14081629>.
- [24] K.L. Hsiao, Micropolar nanofluid flow with MHD and viscous dissipation effects towards a stretching sheet with multimedia feature, *Int. J. Heat Mass Transf.* 112 (2017) 983–990, <https://doi.org/10.1016/j.ijheatmasstransfer.2017.05.042>.
- [25] W.A. Khan, O.D. Makinde, Z.H. Khan, MHD boundary layer flow of a nanofluid containing gyrotactic microorganisms past a vertical plate with Navier slip, *Int. J. Heat Mass Transf.* 74 (2014) 285–291, <https://doi.org/10.1016/j.ijheatmasstransfer.2014.03.026>.
- [26] K. Bhattacharyya, S. Mukhopadhyay, G.C. Layek, I. Pop, Effects of thermal radiation on micropolar fluid flow and heat transfer over a porous shrinking sheet, *Int. J. Heat Mass Transf.* 55 (2012) 2945–2952, <https://doi.org/10.1016/j.ijheatmasstransfer.2012.01.051>.
- [27] S.A. Al-Sanea, Mixed convection heat transfer along a continuously moving heated vertical plate with suction or injection, *Int. J. Heat Mass Transf.* 47 (2004) 1445–1465, <https://doi.org/10.1016/j.ijheatmasstransfer.2003.09.016>.
- [28] I. Waini, A. Ishak, I. Pop, Hybrid nanofluid flow towards a stagnation point on an exponentially stretching/shrinking vertical sheet with buoyancy effects, *Int. J. Numer. Methods Heat Fluid Flow* 31 (1) (2021) 216–235, <https://doi.org/10.1108/HFF-02-2020-0086>.
- [29] S. Dinarvand, M.N. Rostami, An innovative mass-based model of aqueous zinc oxide-gold hybrid nanofluid for von Kármán’s swirling flow, *J. Therm. Anal. Calorim.* 138 (2019) 845–855, <https://doi.org/10.1007/s10973-019-08127-6>.
- [30] N. Ch. Roy, Mathematical approach of demarcation of dual solutions for a flow over a shrinking surface, *Chin. J. Phys.* 68 (2020) 514–532, <https://doi.org/10.1016/j.cjph.2020.10.003>.
- [31] H.A. Nabwey, A. Mahdy, Transient flow of micropolar dusty hybrid nanofluid loaded with Fe<sub>3</sub>O<sub>4</sub>-Ag nanoparticles through a porous stretching sheet, *Results Phys.* 21 (2021) 103777, <https://doi.org/10.1016/j.rinp.2020.103777>.
- [32] S. Dinarvand, M. Nademi Rostami, Three-dimensional squeezed flow of aqueous magnetite-graphene oxide hybrid nanofluid: a novel hybridity model with analysis of shape factor effects, *J. Process Mech. Eng.* 234 (2020) 193–205, <https://doi.org/10.1177/0954408920906274>.
- [33] A. Ghasemian, S. Dinarvand, A. Adamian, M.A. Sheremet, Unsteady general three-dimensional stagnation point flow of a Maxwell/Buongiorno Non-Newtonian nanofluid, *J. Nanofluids* 8 (2019) 1544–1559, <https://doi.org/10.1166/jon.2019.1701>.
- [34] U. Khan, A. Zaib, S.A. Bakar, A. Ishak, Stagnation-point flow of a hybrid nanofluid over a non-isothermal stretching/shrinking sheet with characteristics of inertial and microstructure, *Case Stud. Therm. Eng.* 26 (2021) 101150, <https://doi.org/10.1016/j.csite.2021.101150>.
- [35] N.C. Roşca, I. Pop, Boundary layer flow past a permeable shrinking sheet in a micropolar fluid with a second order slip flow model, *Eur. J. Mech. B/Fluids* 48 (2014) 115–122, <https://doi.org/10.1016/j.euromechflu.2014.05.004>.
- [36] J. Peddieson, An application of the micropolar fluid model to the calculation of turbulent shear flow, *Int. J. Eng. Sci.* 10 (1972) 23–32, [https://doi.org/10.1016/0020-7225\(72\)90072-9](https://doi.org/10.1016/0020-7225(72)90072-9).
- [37] N. Ch. Roy, L.K. Saha, M. Sheikholeslami, Heat transfer of a hybrid nanofluid past a circular cylinder in the presence of thermal radiation and viscous dissipation, *AIP Adv.* 10 (2020) 095208, <https://doi.org/10.1063/5.0021258>.
- [38] A. Saeed, P. Kumam, S. Nasir, et al., Non-linear convective flow of the thin film nanofluid over an inclined stretching surface, *Sci. Rep.* 11 (2021) 18410, <https://doi.org/10.1038/s41598-021-97576-x>.
- [39] T.A.M. Shatanawi, N. Abbas, W. Shatanawi, Mathematical analysis of unsteady stagnation point flow of radiative Casson hybrid nanofluid flow over a vertical Riga sheet, *Mathematics* 10 (2022) 3573, <https://doi.org/10.3390/math10193573>.
- [40] A. Taqi, M. Shatanawi, N. Abbas, W. Shatanawi, Comparative study of Casson hybrid nanofluid models with induced magnetic radiative flow over a vertical permeable exponentially stretching sheet, *AIMS Math* 7 (12) (2022) 20545–20564, <https://doi.org/10.3934/math.20221126>.
- [41] F. Kreith, R.M. Manglik, M.S. Bohn. *Principles of Heat transfer*, Seventh edition, Cengage Learning, 2013.
- [42] F.M. White. *Viscous Fluid Flow*, Third edition, McGraw-Hill, 2006.
- [43] I. Waini, A. Ishak, I. Pop, Hiemenz flow over a shrinking sheet in a hybrid nanofluid, *Results Phys* 19 (2020) 103351, <https://doi.org/10.1016/j.rinp.2020.103351>.
- [44] S. Nasir, A.S. Berrouk, A. Aamir, T. Gul, Significance of chemical reactions and entropy on Darcy-Forchheimer flow of H<sub>2</sub>O and C<sub>2</sub>H<sub>6</sub>O<sub>2</sub> conveying magnetized nanoparticles, *Int. J. Thermofluids* 17 (2023) 100265, <https://doi.org/10.1016/j.ijft.2022.100265>.
- [45] L.F. Shampine, I. Gladwell, S. Thompson. *Solving ODEs with MATLAB*, Cambridge University Press, 2003.

- [46] N.S. Anuar, N. Bachok, Double solutions and stability analysis of micropolar hybrid nanofluid with thermal radiation impact on unsteady stagnation point flow, *Mathematics* 9 (2021) 276, <https://doi.org/10.3390/math9030276>.
- [47] A.H. Mahmoudi, M. Shahi, F. Talebi, Effect of inlet and outlet location on the mixed convective cooling inside the ventilated cavity subjected to an external nanofluid, *Int. Commun. Heat Mass Transf.* 37 (8) (2010) 1158–1173, <https://doi.org/10.1016/j.icheatmasstransfer.2010.04.004>.
- [48] S. Dinarvand, H. Berrehal, I. Pop, A.J. Chamkha, Blood-based hybrid nanofluid flow through converging/diverging channel with multiple slips effect: a development of Jeffery-Hamel problem, *Int. J. Numer. Methods Heat Fluid Flow* 33 (3) (2023) 1144–1160, <https://doi.org/10.1108/HFF-08-2022-0489>.
- [49] S.R. Mishra, I. Khan, Q.M. Al-mdallal, T. Asifa, Free convective micropolar fluid flow and heat transfer over a shrinking sheet with heat source, *Case Stud. Therm. Eng.* 11 (2018) 113–119, <https://doi.org/10.1016/j.csite.2018.01.005>.
- [50] A. Mahmood, B. Ch, A. Ghaffari, Hydromagnetic Hiemenz flow of micropolar fluid over a nonlinearly stretching/shrinking sheet: dual solutions by using Chebyshev Spectral Newton Iterative Scheme, *J. Magn. Magn. Mater.* 416 (2016) 329–334, <https://doi.org/10.1016/j.jmmm.2016.05.001>.
- [51] S. Nasir, S. Sirisubtawee, P. Juntharee, et al., Heat transport study of ternary hybrid nanofluid flow under magnetic dipole together with nonlinear thermal radiation, *Appl. Nanosci.* 12 (2022) 2777–2788, <https://doi.org/10.1007/s13204-022-02583-7>.
- [52] S. Dinarvand, A. Mahdavi Nejad, Off-centered stagnation point flow of an experimental-based hybrid nanofluid impinging to a spinning disk with low to high non-alignments, *Int. J. Numer. Methods Heat Fluid Flow* 32 (8) (2022) 2799–2818, <https://doi.org/10.1108/HFF-09-2021-0637>.
- [53] S. Dinarvand, S.M. Mousavi, M. Yousefi, M. Nademi Rostami, MHD flow of MgO-Ag/water hybrid nanofluid past a moving slim needle considering dual solutions: an applicable model for hot-wire anemometer analysis, *Int. J. Numer. Methods Heat Fluid Flow* 32 (2) (2022) 488–510, <https://doi.org/10.1108/HFF-01-2021-0042>.
- [54] N.A. Khan, S. Khan, A. Ara, Flow of micropolar fluid over an off centered rotating disk with modified Darcy's law, *Propuls. Power Res.* 6 (4) (2017) 285–295, <https://doi.org/10.1016/j.jprr.2017.11.006>.